Journal of Water Process Engineering 64 (2024) 105623

Contents lists available at ScienceDirect

Journal of Water Process Engineering

journal homepage: www.elsevier.com/locate/jwpe

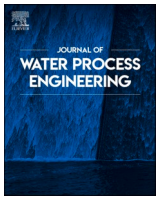

Challenges in the determination of reactive oxygen species evolving during membrane water electrolysis for *in situ* ozone production

Roman Grimmig [a,b,*], Philipp Gillemot [a], Axel Kretschmer [a], Klaus Günther [c], Helmut Baltruschat [d], Steffen Witzleben [a]

[a] Bonn-Rhein-Sieg University of Applied Sciences, Department of Natural Sciences, von-Liebig-Str. 20, 53359 Rheinbach, Germany
[b] Innovatec Gerätetechnik GmbH, von-Liebig-Str. 6, 53359 Rheinbach, Germany
[c] Research Centre Jülich, Institute for Bio- and Geosciences (IBG-2), Wilhelm-Johnen-Straße, 52428 Jülich, Germany
[d] University of Bonn, Clausius Institute for Physical and Theoretical Chemistry, Römerstr. 164, 53117 Bonn, Germany

ARTICLE INFO

Editor: Guangming Jiang

Keywords:
Hydroxyl radicals
Oxidation-reduction-potential
Ozone generator
PEM water electrolysis
Reactive oxygen species

ABSTRACT

The treatment of ultrapure water with electrochemically produced O_3 is a common means for disinfection yet leads to the formation of a variety of reactive oxygen species (ROS). The present study draws a comprehensive comparison between three commonly used photometric and fluorometric assays for ROS analysis and quantifies the individual signal responses for dissolved O_3, ·OH and H_2O_2, respectively, to account for cross-sensitivities. By calibrating all combinations of assays and analytes, we developed a quantification procedure to reliably determine the actual ROS composition in ultrapure water environments for different operation conditions of a membrane water electrolyzer with PbO_2 anodes down to concentrations of 0.97 µg L^{-1}. While the ·OH formation rate can be described linearly over the observed current density range, substantial O_3 evolution is only found for current densities of 0.75 A cm^{-2} and above (up to 3.7 µmol h^{-1} for J = 1.25 A cm^{-2}). The formation of H_2O_2 is only observed when an organic carbon source is introduced into the solution. We further quantify the interference of H_2O_2 with the reading of the oxidation-reduction potential as a common water parameter and elaborate on its validity to monitor the peroxone process when both H_2O_2 and O_3 are present simultaneously.

1. Introduction

Water supply lines are critical infrastructure elements that have to be kept free from pathogens and pollutants in order to provide access to potable or process water in suitable qualities for the intended applications. The necessity for their systematic sanitization becomes most obvious when considering cold-stored ultrapure water, *e.g.* for pharmaceutical purposes [1,2]. Typically, disinfection is achieved by adding oxidants at defined levels to the water feed to inactivate harmful microorganisms and remove contaminations effectively [3–5]. While potable water is still commonly treated with different chlorine species, the formation of potentially critical disinfection by-products has to be avoided and therefore O_3 constitutes the preferred powerful oxidant ($E^0(O_3/O_2) = +2.07$ V *vs.* SHE) for use in ultrapure water environments [6,7].

As the necessary amount of oxidant varies greatly depending on both the feed water quality and the required water conditions, it is desirable to adopt the introduction of O_3 into the feed water in a defined manner. Since this unstable compound cannot be conveniently stored in gas cylinders, a frequently suggested approach for disinfection and continuous removal of residual organic compounds is based on the *in situ* formation of reactive oxidants (*i.e.* ·OH or O_3) by direct oxidation of water. As their evolution occurs at higher thermodynamic potentials than oxygen gas, there is a state of competition between the oxygen evolution reaction (OER) and *e.g.* the electrochemical ozone production (EOP) [8]. Therefore, the use of special electrocatalysts, such as boron-doped diamond (BDD) or β-PbO_2 with a high overvoltage for oxygen evolution, is indispensible for an efficient anodic oxidation [9–12]. During this process water is split into both hydrogen gas and a mixture of O_2 and O_3 gasses by electrical energy using a thin, solid polymer electrolyte membrane (PEM) as an ionic conductor between the electrodes [13,14]. This favorable design does not depend on the electrical conductivity of the ultrapure water, which is often a limiting characteristic for electrolysis.

The mechanism of the electrochemical O_3 generation strongly depends on the selected electrocatalyst and involves the formation of ·OH

* Corresponding author at: Bonn-Rhein-Sieg University of Applied Sciences, Department of Natural Sciences, von-Liebig-Str. 20, 53359 Rheinbach, Germany.
E-mail address: roman.grimmig@h-brs.de (R. Grimmig).

https://doi.org/10.1016/j.jwpe.2024.105623
Received 26 February 2024; Received in revised form 23 May 2024; Accepted 6 June 2024
Available online 13 June 2024

as precursor species, which may be either strongly adsorbed for subsequent surface reactions (*e.g.* on β-PbO_2) or weakly adsorbed and partially released (*e.g.* on BDD) [15,16]. Current efficiencies for O_3 evolution of up to 20 % for PbO_2 and 42 % for BDDs were reported during membrane water electrolysis, although these values have shown to strongly depend on the operational conditions and electrocatalyst stoichiometry [17,18]. Depending on the feed quality, not all O_3 is immediately consumed during water treatment, with the remainder contributing to a systemic protection of stored ultrapure water due to a depot effect.

The decomposition of O_3 is a complex interaction of reactive oxygen species (ROS) with each other. Due to the short half-life of dissolved O_3 ($t_{1/2} \approx 80$ min in an ultrapure water setting under similar conditions [19]), it decays rapidly and can generate a large amount of ·OH [20–22], which are highly reactive (E^0(·OH/H_2O) = +2.73 V *vs.* SHE [23]) and enable further secondary oxidation reactions, especially with (organic) contaminants [11,24–26]. Although many involved intermediate species have a chemically instable character, by-products such as H_2O_2 can be quantitatively determined, especially when they emerge during the ozonation of dissolved organic matter [27–29]. However, as H_2O_2 is known to rapidly decompose O_3 *via* the peroxone reaction [30], its accumulation in ultrapure water systems may impede the overall sanitization process due to its impact on the systemic protection. Because of this multi-step reaction cascade including many short-lived intermediates, there may be a variety of ROS present in solution, which contribute to the overall disinfection effect. An overview of evolving ROS in a PEM electrolyzer setup is given in Fig. 1, depicting a selection of the most prominent reactions within the O_3 degradation cascade. The O_3 evolution process (orange and yellow area) emphasizes the competition between OER and EOP, depending on the surface coverage of oxygen intermediates. The following, non-exhaustive decomposition cycle (blue area) integrates a broad variety of short-lived radicals, which can also lead to H_2O_2 as a stable oxidizing agent.

As a common and convenient technique to characterize the oxidative properties of water samples, the oxidation-reduction potential (ORP) should allow for an estimation of the present disinfectant concentration [31,32]. However, in systems which inherently allow for the presence of more than one ROS, the ORP signal is a mere sum parameter and may camouflage inconsistent water quality levels due to varying ROS compositions [33]. Hence, for applications demanding detailed information about the concentration of individual ROS, measuring the ORP signal cannot be the method of choice.

In addition to the presence of electrochemically produced O_3, other ROS can emerge in aqueous solution and therefore pose a particular challenge for independent quantification [34,35]. Concerning dissolved O_3 as the target analyte, electrochemical sensor systems that enable measurements in a range of 0.5 to 200 µg L^{-1} [19,36,37] have been developed and proven reliable in automated process analytics. Simple colorimetric assays (based on dyes such as DPD or Indigo) are still commonly applied as convenient off-line analyses in laboratory and field trials and can detect O_3 as low as 0.4 to 40 µg L^{-1} [38–40], but are known to also react with other oxidizing species [41–43]. As for ·OH, common quantification approaches involve rapid reactions of radical scavengers (*e.g.* terephthalic acid), followed by a subsequent analysis of the reaction products *via* chromatography [44,45], UV spectrometry [46,47], fluorescence [48–50] or even electron spin resonance [51]. For a selective determination of H_2O_2, a variety of colorimetric and electrochemical methods [52–54] can be used, including the most prominent titanyl sulfate assay [55].

While these advanced analytical methods ensure a highly selective and sensitive determination of ROS, they can only be applied in well-equipped laboratory settings. In contrast, it is common knowledge that quick routine analyses by colorimetric assays suffer from considerable cross-sensitivities when multiple ROS occur simultaneously, although these distortions have been insufficiently characterized.

In this study we provide insight into the three most common colorimetric assays used for the quantification of the three most prominent reactive oxygen species evolving during the ozonation of water *via* electrolysis, namely O_3, ·OH and H_2O_2 *via* DPD, $TiOSO_4$ and terephthalic acid. With this approach, a stepwise procedure is presented to quantify the actual ROS composition with respect to cross-sensitivities between the evaluated assays. Following our findings, we provide a holistic view on the resulting oxidant composition for different operational conditions of a PEM electrolyzer setup with PbO_2 anodes intended for O_3 evolution.

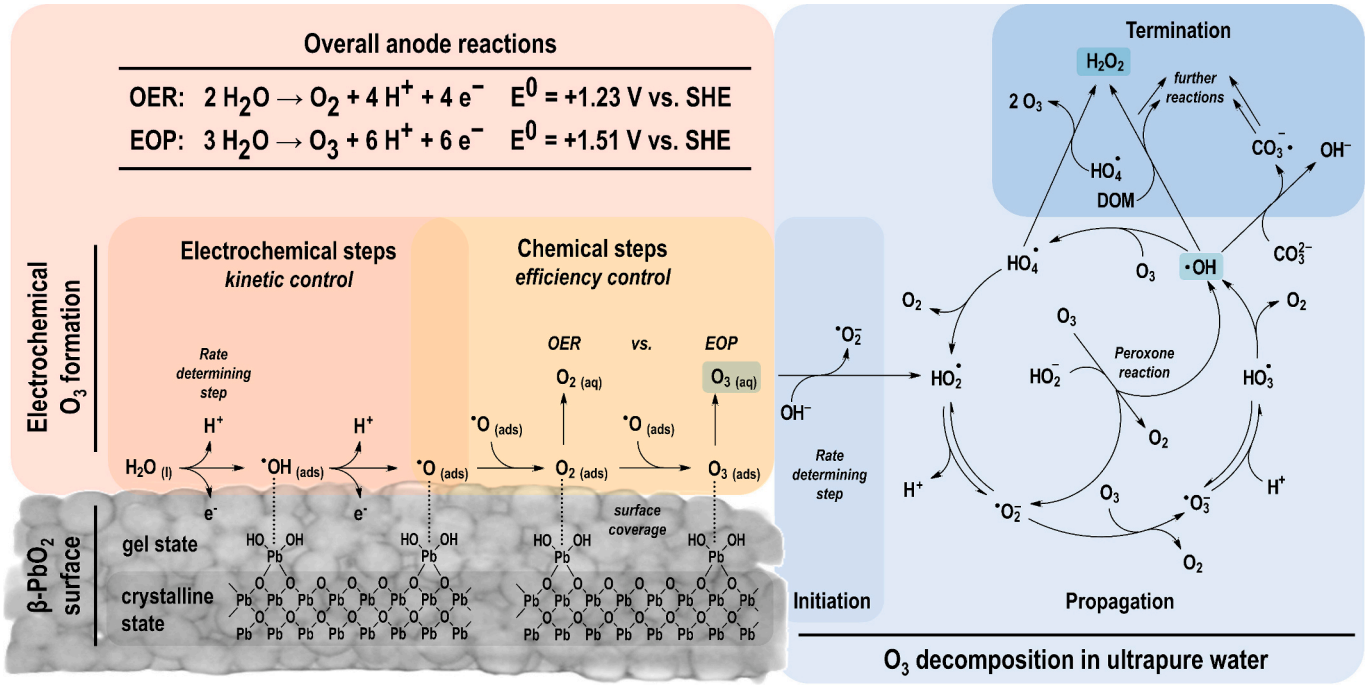

Fig. 1. Scheme of the evolution of different ROS during PEM electrolysis on a β-PbO_2 anode surface and subsequent decomposition of O_3 in ultrapure water. Own drawing, adapted and combined according to [8,27,30,78–82].

Furthermore, we elaborate on linking the chemical information about the ROS composition from colorimetric assays with the analytical water parameters ORP and TOC (total organic carbon).

2. Materials and methods

2.1. Experimental setup

To investigate the evolution of ROS during the operation of a commercial PEM water electrolyzer, the setups depicted in Fig. 2 (similar to previously published studies [56,57]) were used for all experiments. Within a water reservoir, an Ozone-Micro-Cell (OMZ CH1) was installed as the O_3 evolving unit, consisting of one PbO_2-coated porous titanium anode and one porous stainless-steel cathode (all Innovatec Gerätetechnik GmbH, Rheinbach, Germany), and separated by a Nafion™ 117 membrane (Chemours®, Wilmington, Delaware, USA) in a membrane-electrode assembly (MEA) setup. Nafion™ was chosen due to its high chemical stability while maintaining a low electrical resistance in the electrolyzer setup. Simultaneously, it acts as a proton conducting ionomer, thus enabling the PEM function principle.

For experiments with "indirect" ozonation, the evolving gases were exhausted through a stainless-steel pipe into a separate ultrapure water reservoir to evaluate O_3 evolution selectively without the presence of ROS generated by side-reactions. "Direct" ozonation refers to ultrapure water in the reaction vessel being treated electrochemically without mediation, which was selected for the investigation of ·OH and H_2O_2 evolution.

Evolving oxidizing agents were investigated over 90 min of operation and current densities in a range from 0.25 to 1.25 A cm^{-2}, referring to a geometric surface of 0.2 cm^2 for the anode. In order to simulate a typical stand-by operation, an additional level of 0.01 A cm^{-2} (for anodic protection of the catalytically active PbO_2 layer) was evaluated. All reported data for every experimental condition are mean values originating from three independent replicate runs.

For certain experiments, isopropyl alcohol (denoted i-PrOH; Carl Roth, Karlsruhe, Germany) was added to the ultrapure water to achieve defined levels of dissolved organic matter, represented by the TOC value as a common analytical water parameter. Concentrations were adjusted within a range between 0 and 1 mg L^{-1}, which is in congruence with previous studies [58]. In order to mitigate effects caused by light or CO_2 ingestion, these experiments were conducted under Argon 4.8 gas purging (Westfalen AG, Münster, Germany) and UV protection.

2.2. Analytical procedures

For each of the three analytes, an individual assay is used to quantify concentrations and production rates, and additionally tested for cross-sensitivities. For this purpose, the assays were equally treated with defined concentrations of the other ROS under investigation, aiming to describe the signal response with suitable regression functions. The chosen analytical procedures yield observable concentrations for dissolved O_3 and H_2O_2, however, only a cumulative value for scavenged ·OH can be obtained due to its extremely short-lived character ($\tau \approx 10$ µs) [59].

Determination of O_3 was carried out using the DPD assay in accordance with DIN 38408-3:2011-04, using DPD ((N,N)-diethyl-p-phenylenediamine; Fisher Scientific, Waltham, MA, USA), KIO_3 (Merck, Berlington, MA, USA) as well as KI and Na_2SO_3 (both Carl Roth, Karlsruhe, Germany) [41]. O_3 reacts with DPD in a one-electron transfer reaction, forming a radical DPD cation acting as a detectable dye. After 1 min the absorption of the magenta radical cation can be measured at $\lambda_{max} = 510$ nm. For different concentration ranges, 1 cm and 5 cm cuvettes were used.

Hydroxyl radical formation was evaluated with a fluorometric method according to [49] using terephthalic acid (TA) (Alfa Aesar, Haverhill, MA, USA) and 2-hydroxyterephthalic acid (HTA) (Apollo Scientific, Bredbury, United Kingdom). Hydroxyl radicals are scavenged by TA forming HTA, which can be measured by excitation at $\lambda_{max} = 312$ nm and subsequent detection of fluorescence at $\lambda_{max} \approx 430$ nm. HTA calibration solutions in the range from 0.11 to 3.64 mg L^{-1} as well as analyte solutions were excited and the resulting fluorescence signal was used for characterization. Fluorescence spectra were processed with OriginPro 2022 (OriginLab, Northhampton, MA, USA) by integration of the acquired fluorescence signal between $\lambda = 340$ nm and $\lambda = 580$ nm and background correction. For cross-sensitivity evaluation of the DPD assay, the amount of ·OH was adjusted using H_2O_2 and $FeSO_4 \cdot 7\ H_2O$ (both Carl Roth, Karlsruhe, Germany) via Fenton reaction.

The quantification of H_2O_2 was carried out based on DIN 38409-15:1987-06 using a solution of titanyl sulfate in sulfuric acid (Merck, Berlington, MA, USA) in a 5 cm cuvette [60]. Ti^{4+} ions form colorless aquo complexes which turn into yellow complex cations by ligand exchange after the addition of H_2O_2. Within 5 min, the absorption is measured at $\lambda_{max} = 407$ nm. Calibration solutions were prepared ranging from 0.07 to 1.77 mg L^{-1}.

All chemicals were at least of analytical grade purity. 18.2 MΩ ultrapure water was provided for all experiments by a ELGA Purelab Flex (VWS, High Wycombe, UK) water purification system. Photometric determinations were performed on a DR3900 UV/VIS spectral photometer (Hach Lange, Loveland, CO, USA). For fluorometric determinations, a custom setup was developed using SETi (Columbia, SC, United States) CUD1GF1A light emitting diodes ($\lambda_{max} = 315$ nm) and an Ocean Insight (Orlando, FL, United States) Ocean HDX spectrometer. A comprehensive overview of all applied assays for ROS determination in this study is given in Fig. 3.

2.3. ORP measurements

For ORP (oxidation-reduction potential) signal measurements, stock solutions of O_3 (approx. 2 mg L^{-1}) and H_2O_2 (approx. 100 mg L^{-1}) were freshly prepared. Solutions in a range of $\beta_{aq}(O_3) = 0.2$ mg L^{-1} to 1.0 mg

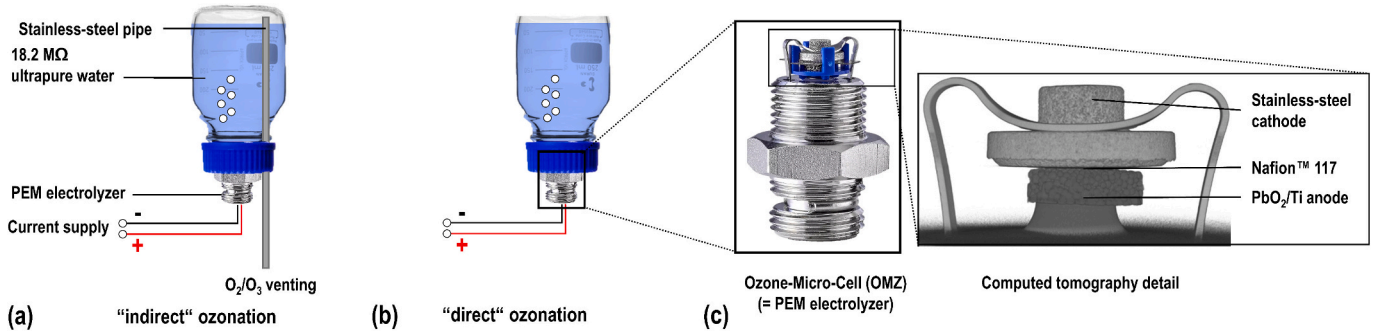

Fig. 2. Scheme of the experimental setup for **(a)** "indirect" ozonation and **(b)** "direct" ozonation of water reservoirs. **(c)** A detailed insight into the MEA arrangement and its porous electrodes is given using computed tomography imaging.

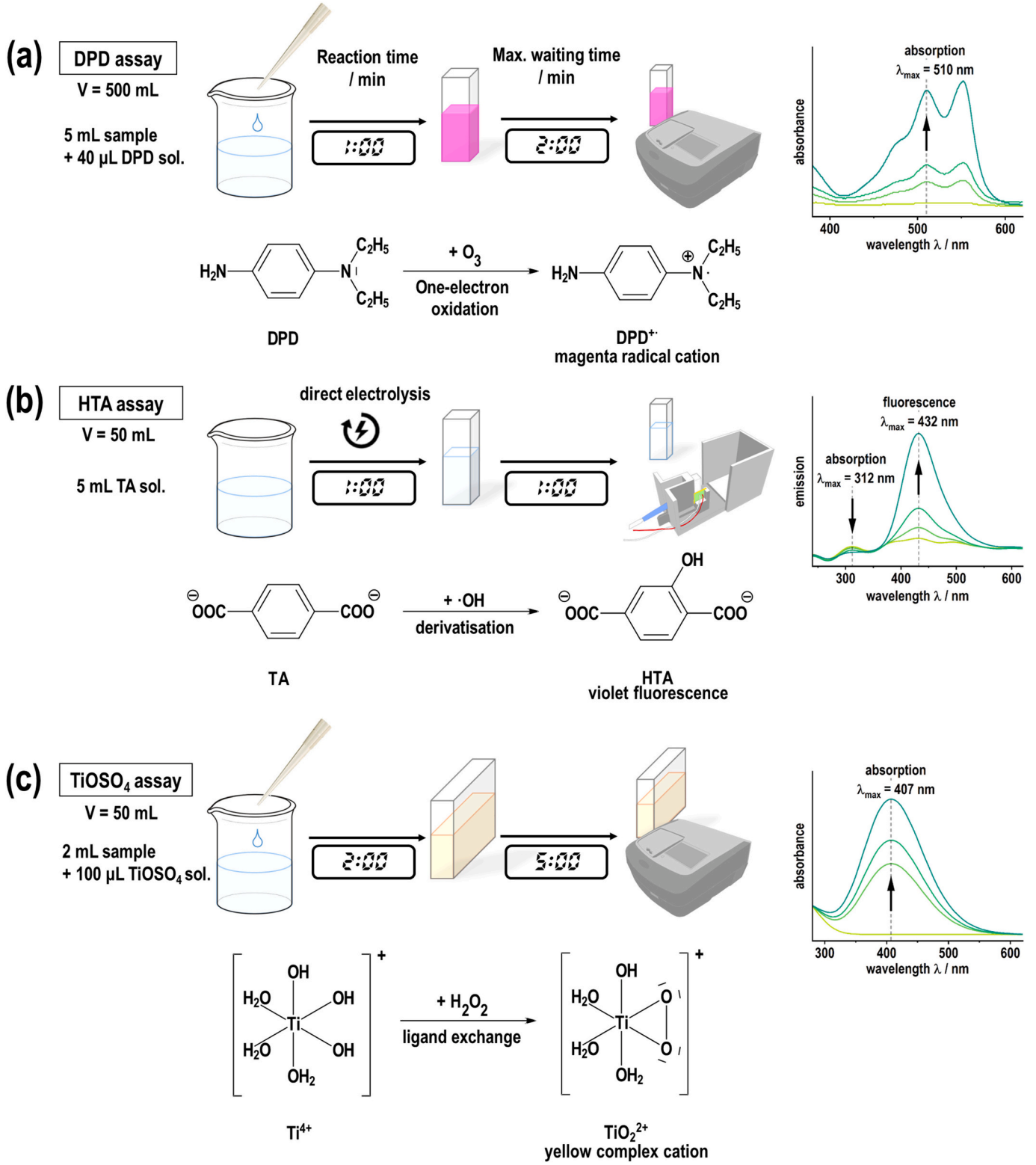

Fig. 3. Overview of the assays for ROS determination used in this study: **(a)** O_3 determination *via* DPD assay. **(b)** ·OH determination *via* HTA assay. **(c)** H_2O_2 determination *via* $TiOSO_4$ assay.

L^{-1} and $\beta_{aq}(H_2O_2) = 0.1$ mg L^{-1} to 17 mg L^{-1} were measured with a SenTix® Pt ORP sensor equipped with a Ag/AgCl reference electrode (Xylem Analytics, Washington, D.C., US) and an InLab Micro pH electrode (Mettler Toledo, Columbus, OH, US). Concentrations were verified using the aforementioned colorimetric assays intended for the respective analytes.

In order to evaluate the consumptive effect of H_2O_2 on dissolved O_3, a reaction vessel with 5 L of ozonated water at different concentrations ($\beta_{aq}(O_3) = 50$ and 100 µg L^{-1}) was prepared via "indirect" ozonation and subsequently doped with different levels of H_2O_2 in a molar ratio range of $n_0(H_2O_2)/n_0(O_3) = 0.14$ to 13.5. ORP values were evaluated with a 1 Hz data acquisition rate over a time of 10 min before and after H_2O_2

addition to determine the occurring signal drop.

3. Results and discussion

3.1. Evaluation of the analytical performance of colorimetric ROS determination methods and their cross-sensitivities

In order to assess the reliability of the obtained spectroscopic data in a first step, all selected methods were examined with respect to the analytical performance of the conducted calibrations. Therefore, limits of detection (LOD) and quantification (LOQ) as well as the coefficient of variation of the procedure (V_{x0}) were evaluated for all analytes of interest using the calibration approach according to DIN ISO 11843-2:2006-06 and DIN 32645:2008-11 (see supplementary material, Table S1). All values are expressed as both a mass and molar concentration to give a tangible value for practitioners and also allow for a direct comparison in relative response per reactive oxygen species.

All calibrations were fitted to linear functions with coefficients of determination $R^2 \geq 0.9995$ and precision coefficients of <2.3 %, yielding LOD values as low as 0.97 µg L^{-1} for O_3. Given that all species under investigation can be quantified to trace concentrations of <2.72 µmol L^{-1}, monitoring of all oxygen species during PEM electrolysis is confidently possible. This especially holds true for applications in technical facilities where O_3 concentrations between 0.35 and 1.15 µmol L^{-1} are favorably applied [7]. Due the nature of the HTA assay, the obtained analytical parameters only refer to accumulated amounts of scavenged ·OH instead of actual ·OH concentrations.

As stated before, many colorimetric assays chosen for the determination of ROS are not necessarily selective to a single species. In order to evaluate cross-sensitivities, the assay response matrix for all investigated ROS is given in Fig. 4, with the relevant calibration features listed in Table 1. For O_3 determination *via* DPD, two separated calibration curves are obtained as two different cuvette sizes are used depending on the concentration range.

Not only can valid calibrations be obtained for the assays which are intended for the respective species, it is also possible to adequately describe all observable cross-sensitivities in the observed concentration range by simple regression models: Either the regression yields a linear function when there is a significant reaction or the measured, constant signal is independent of the species concentration, leading to a horizontal line as the assay does not respond to the respective ROS.

If ROS are to be determined without the presence of interfering species, the intended assays exhibit their suitability. As all calibrations refer to molar concentrations, it is possible to compare the sensitivity for each ROS and method by comparing the slopes of the regression functions. For instance, the quantification of H_2O_2 is most sensibly carried out using the $TiOSO_4$ assay, which is more than four times more sensitive to H_2O_2 than the alternative DPD assay (3.569 *vs.* 0.803 L $mmol^{-1}$).

Table 1
Regression parameters for the linear models describing the assay responses for the respective ROS. Regression functions and R^2 values are given for each analyte and assay combination, except for calibrations yielding no concentration dependence. I stands for the signal absorbance or fluorescence (both in arbitrary units, denoted a.u.) and c_{aq} refers to the molar ROS concentration.

Analyte	Assay	Regression function	Linearity
O_3	DPD (1 cm cuvette)	$I = 13.5 \bullet c_{aq} + 0.008$	$R^2 = 0.9995$
	DPD (5 cm cuvette)	$I = 97.1 \bullet c_{aq} + 0.001$	$R^2 = 0.9999$
	HTA	$I = 4.51 \bullet 10^6 \bullet c_{aq} + 0.02 \bullet 10^6$	$R^2 = 0.9773$
	$TiOSO_4$	$I = 0.000$	n.a.
·OH	DPD	$I = 1.30 \bullet c_{aq} + 0.012$	$R^2 = 0.9942$
	HTA	$I = 26.2 \bullet 10^6 \bullet c_{aq}$	$R^2 = 0.9998$
	$TiOSO_4$	n.a.	n.a.
H_2O_2	DPD	$I = 0.803 \bullet c_{aq} + 0.003$	$R^2 = 0.9946$
	HTA	I = 0.000	n.a.
	$TiOSO_4$	$I = 3.569 \bullet c_{aq} + 0.003$	$R^2 = 0.9997$

For ·OH formation the application of the HTA assay is indicated as only the DPD assay leads to measurable results despite being quite insensitive. This observation is similar to a related work, where DPD was used as a radical detection assay involving a Fenton reaction by adding H_2O_2 into a Fe(II)-containing DPD solution, leading to a more pronounced sensitivity [43]. As ·OH is generated from H_2O_2 *via* the Fenton reaction for calibration, evaluating the signal of the $TiOSO_4$ assay would be unselective and misleading. For a selective evaluation of ·OH *via* the $TiOSO_4$ assay, it would be necessary to reproducibly provide defined amounts of ·OH without using H_2O_2 as a source. Furthermore, the resulting red complex contains a ligand with a peroxide group, which is highly unlikely to form by ·OH self-recombination. Other radical scavenging assays such as ABTS [61] or chromotropic acid [62] were evaluated in pretrials but have proven to not be applicable for species-selective determinations in ozonated water when more than one ROS is present. In case of O_3 determination, both the DPD and HTA assay can be used with sufficient sensitivity, although the reaction from TA to fluorescing HTA is known to be caused by O_3 decay and subsequent radical liberation and not by direct ozonation [63,64].

As multiple ROS may be able to coexist within an ultrapure water distribution system due to spatial and temporal separations, the contributions of different species may lead to similar signal responses if only one detection method is applied. Choosing an appropriate and

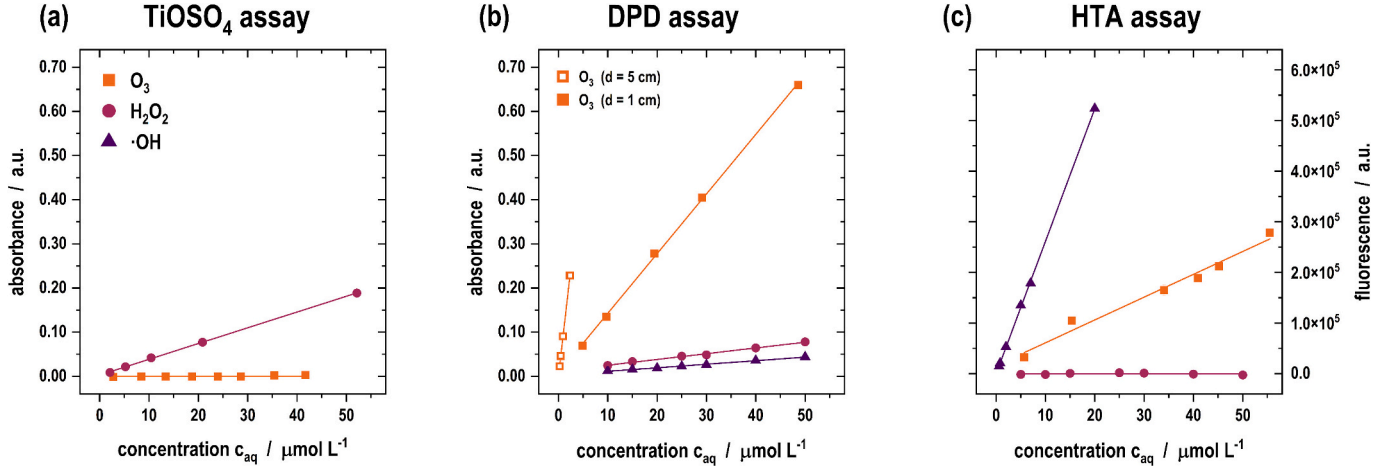

Fig. 4. Overview of the responses for the **(a)** $TiOSO_4$ assay, **(b)** DPD assay and **(c)** HTA assay to identify cross-sensitivities. The absorbance for both the $TiOSO_4$ and DPD assay is given on the left axis while the fluorescence signal of the HTA assay is referred to on the right axis. Error bars are included, but mostly invisible as they are smaller than the symbol size.

representative sampling point is therefore both tricky and crucial, as varying ROS compositions will not yield unambiguous determinations. This is especially true for highly reactive species that can interact with contaminants or even other ROS.

When it comes to the quantification of more than one occurring ROS, a sensitive determination of O_3 can be achieved by applying the standardized, well-known Indigo assay [38,41], which showed no considerable cross-sensitivity for H_2O_2 in pretrials of this study. However, this assay proved to be only applicable in a calibration range from 0.1 up to 0.3 mg L^{-1} O_3 for the available spectrophotometer equipped with a 5 cm cuvette. Therefore, this assay was not used for subsequent O_3 quantifications in this study, which required lower LOD and LOQ values as well as a higher method precision to confidently monitor O_3 evolution. Nevertheless, for similar applications dealing with an O_3 concentration that is consistent with the calibration range provided by the Indigo assay, this approach could be beneficially applied. If the quantification of H_2O_2 is desired in the presence of other ROS, the $TiOSO_4$ assay is the preferred method, as no interference with O_3 was observed.

Due to the partial selectivity of the presented assays, a breakdown into distinct ROS concentrations is obscured and requires a correction function by using matrix calculation on a linear system of equations [65]. This is used to separate the individual contributions and calculate amended concentrations which reflect the actual ROS composition at a given sampling point more accurately. Consequently, a stepwise ROS quantification needs to be carried out to obtain a comprehensive analysis.

As the determination of H_2O_2 *via* the $TiOSO_4$ assay is the only method that has proven to be unimpeded by the other ROS under investigation, it inherently provides the real H_2O_2 concentration in a first step (Eq. (1)). Solving the linear system of equations leads to Eq. (2) and Eq. (3) which allow for an amended O_3 quantification in the presence of H_2O_2. Due to the short lifespan of the hydroxyl radical, only a virtual ·OH concentration (representing the cumulated amount of formed radicals in the given reaction vessel) can be determined with this approach by using the quantified interferences for the other species. For the DPD assay only the calibration range for a 1 cm cuvette was considered.

$$\frac{c_{amended}(H_2O_2)}{\frac{mmol}{L}} = 0.280 \bullet I_{TiOSO_4} - 8.41 \bullet 10^{-4} \quad (1)$$

$$\frac{c_{amended}(O_3)}{\frac{mmol}{L}} = -0.0169 \bullet I_{TiOSO_4} - 3.74{\cdot}10^{-9} \bullet I_{HTA} + 0.0753 \bullet I_{DPD} - 0.002 \quad (2)$$

$$\frac{c_{amended}(\bullet OH)}{\frac{mmol}{L}} = 0.0029 \bullet I_{TiOSO_4} + 3.88{\cdot}10^{-8} \bullet I_{HTA} - 0.013 \bullet I_{DPD} - 4.87{\cdot}10^{-4} \quad (3)$$

Since the DPD assay shows a reaction with all ROS under investigation, it can be interpreted as an unspecific sum parameter for all occurring oxidizing agents. While this assay may be sufficient to depict O_3 concentrations at the time of sampling, the determination of exact formation rates for different ROS requires conducting an HTA assay in parallel. Furthermore, if the presence of H_2O_2 cannot be strictly ruled out, an evaluation *via* the $TiOSO_4$ assay is also necessary.

In practice, a parallel determination of all three assays is proposed to achieve the most accurate representation of the ROS composition for any given state of operation. For subsequent ROS quantification in the following sections, these corrections were thusly applied.

3.2. ROS evolution during PEM electrolysis

Operating the PEM electrolyzer in ultrapure water leads to gaseous O_3 evolution on the anodic surface with bubbles eventually rising to the water surface. In this process, O_3 partially dissolves into the ultrapure water and can be detected using the aforementioned methods. Fig. 5(a) shows that the amount of dissolved O_3 increases with the elapsed experimental time and can be described by linear regression functions for all applied current densities.

After an experimental time of 90 min, dissolved O_3 concentrations of 0 μmol L^{-1} and 5.62 μmol L^{-1} were measured for J = 0.01 A cm^{-2} and 1.25 A cm^{-2}, respectively. Even when applying a current density of 0.25 A cm^{-2} only 0.08 μmol L^{-1} were found for the same time frame, which is in a comparable order of magnitude as with the applied protection current alone. This barely traceable increase in O_3 concentration over time is also demonstrated by low R^2 values. However, for elevated current densities, an accelerated increase in dissolved O_3 concentration is observed (see Fig. 5(b)). For J ≥ 0.75 A cm^{-2}, the O_3 formation rate follows a linear trend as indicated by the black dashed line. Presumably, this can be attributed to lower anodic potentials at low current densities, which may be insufficient for a significant O_3 evolution as OER is thermodynamically preferred over EOP.

The obtained formation rates are a direct result of the experimental setup and only refer to the aqueous phase. A substantial amount of O_3 is lost by rising and degassing bubbles, although O_3 exhibits a high solubility in water in direct comparison to O_2 as the main product (480 mg L^{-1} *vs.* 38 mg L^{-1} at 25 °C) [66]. Therefore, a reasonable estimation of a current efficiency is impeded for the given setup. Accounting for a quantitative measurement of both gaseous and aqueous O_3, current efficiencies of 15–20 % were previously reported for ultrapure water electrolysis with PbO_2 anodes in a comparable setup [17,67].

Hydroxyl radicals play an important role in both the electrochemical generation and subsequent decay of O_3. Scavenging allows for a time-resolved monitoring of radical evolution depending on the respective electrolyzer setting as displayed in Fig. 6(a). As TA is known to be resistant to oxidation by O_3 as well as direct electron transfer reactions [64,68], it is a suitable probe for ·OH in this environment and the measured concentration of HTA can therefore be interpreted as an equivalent to the cumulated amount of ·OH.

While for "direct" ozonation no significant radical accumulation (and therefore formation) is observed in stand-by operation, an increase in current density yields notable amounts of scavenged •OH. For all standard operational modes (J ≥ 0.25 A cm^{-2}), the progressively increasing amount of scavenged •OH in solution can be described by linear functions (all R^2 = 0.93 and higher) that allow for a derivation of •OH formation rates during electrolysis. Plotting the so-obtained values as a function of the applied current density (Fig. 6(b)) yields a linear correlation with increasing current densities for both "indirect" and "direct" ozonation (R^2 = 0.975 and 0.972, respectively). As the formation rates for both operational conditions are in similar ranges for each current density level, the occurrence of •OH can be fully explained by the decomposition of dissolved O_3, indicating no electrochemical generation at PbO_2 anodes. This is in accordance with the mechanistical understanding of the electrochemical surface reactions in ultrapure water [16,69]. Minor differences in the measured formation rates of both operational modes may be attributed to temperature effects (*e.g.* by heat dissipation from the electrolyzer), leading to a shorter half-life of O_3.

These observations contrast with the generation of O_3 which required higher current densities. While formation rates $\dot{n}(O_3)$ from 0.07 up to 3.70 μmol h^{-1} were determined for O_3 evolution in the observed current density range, only 0.05 to 0.37 μmol h^{-1} were observed for •OH under the same operation conditions, exhibiting a difference of up to an entire order of magnitude. Considering the ratio $\dot{n}(\bullet OH)/\dot{n}(O_3)$, values between 0.10 and 0.82 are obtained for all standard operational modes and decrease with increasing current densities.

Controlling the operating conditions of a PEM electrolyzer can help mitigate or predict the evolution of unwanted H_2O_2 because of its impact on O_3 depletion. Depending on the structural properties of dissolved carbon sources, various pathways for a reaction with O_3 are possible that lead to the emergence of H_2O_2 as a stable side-product (especially *via* the

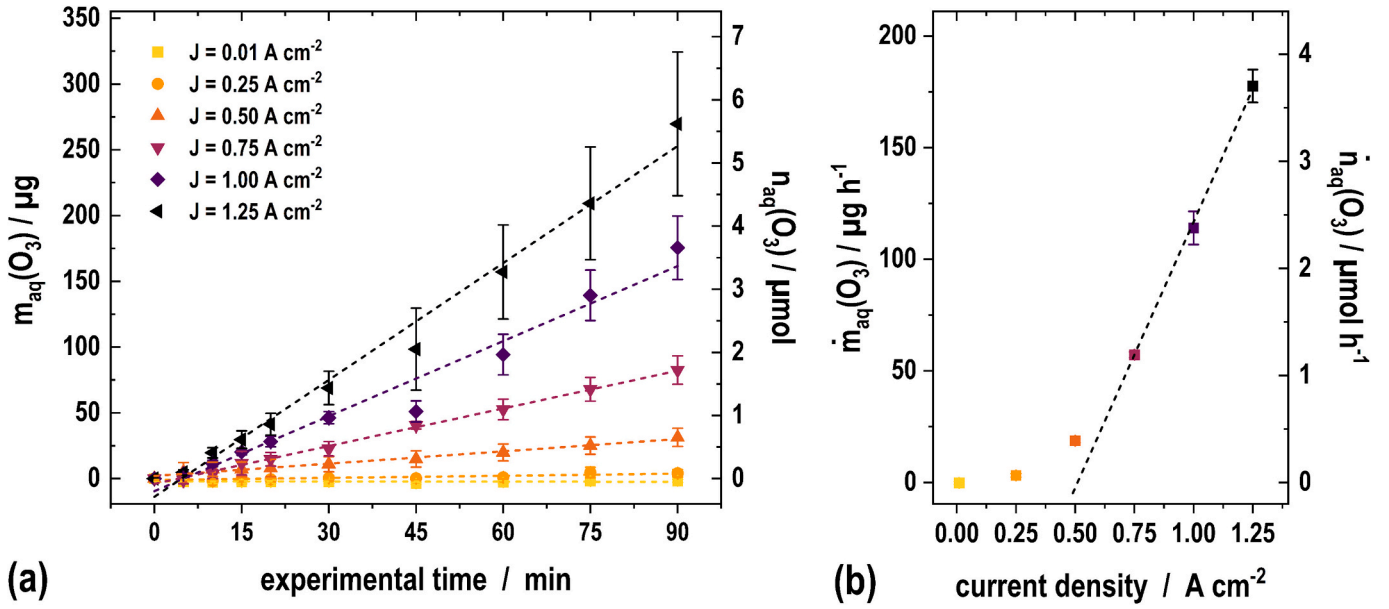

Fig. 5. **(a)** Amount of dissolved $n_{aq}(O_3)$ and $m_{aq}(O_3)$ as a function of the elapsed experimental time for different current densities applied to the electrolytic O_3 generator. **(b)** O_3 formation rates $\dot{m}_{aq}(O_3)$ and $\dot{n}_{aq}(O_3)$ as a function of the applied current density.

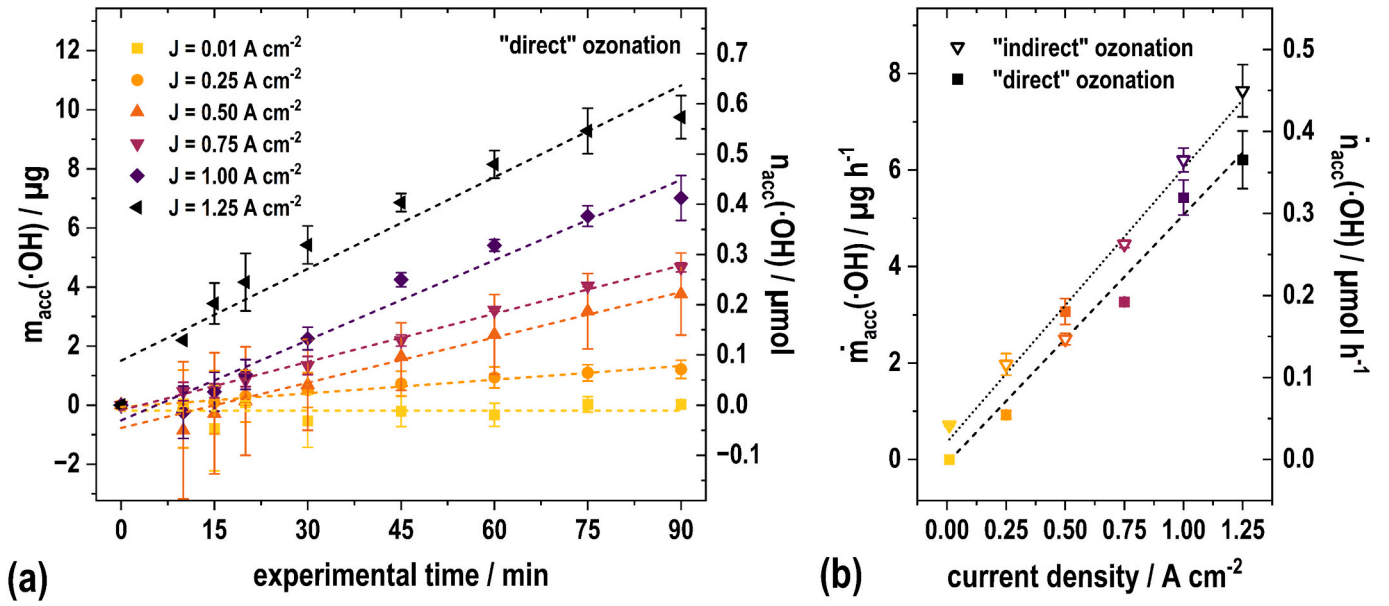

Fig. 6. **(a)** Amount of accumulated $n_{acc}(\bullet OH)$ and $m_{acc}(\bullet OH)$ as a function of the elapsed experimental time for different current densities applied to the PEM electrolyzer. **(b)** The formation rates $\dot{m}_{acc}(\bullet OH)$ and $\dot{n}_{acc}(\bullet OH)$ as a function of the applied current density (black dotted and dashed lines) for both "indirect" ozonation (▽) and "direct" ozonation (■).

Criegee mechanism for unsaturated compounds) [70]. When considering discontinuously operated ultrapure water distribution systems, a common means of disinfection is isopropyl alcohol (i-PrOH), which often cannot be completely rinsed out and is not removed by commonly applied electro de-ionization either [58]. Therefore it remains in trace amounts as a typical carbon source. As not all structural properties can be adequately represented by a single molecule, the selected i-PrOH only serves as one exemplary model substance and does not allow for a generalized extrapolation for other contaminants contributing to the TOC value. However, due to its high radical scavenging capacity ($k = 2.3 \cdot 10^9$ L mol^{-1} s^{-1} [71]) i-PrOH showcases a worst-case estimation for H_2O_2 formation rates in ultrapure water storage and distribution systems.

Specifically for i-PrOH, Reisz et al. have reported a mechanistic scheme for both O_3 and ·OH mediated pathways that indicate a H_2O_2 yield of about 1.5 % considering a non-electrochemical ozonation [27]. The formation rates of H_2O_2 in the presence of i-PrOH are shown in Fig. 7 as a function of time, current density and TOC level.

As the increase in H_2O_2 concentration also follows a linear trend with time ($R^2 > 0.95$ for all experiments), formation rates were obtained in the same manner as for the other ROS. The progression of measured H_2O_2 concentration over the course of the experimental time is exemplarily depicted in Fig. 7(a) (inset graph) for $J = 1.00$ A cm^{-2} and β_{aq}(i-PrOH) = 0.50 mg L^{-1}. Keeping the initial TOC level at a constant value of 0.50 mg L^{-1}, the resulting formation rates $\dot{m}_{aq}(H_2O_2)$ and $\dot{n}_{aq}(H_2O_2)$ increase linearly with elevated current densities from 3.9 ± 2.6 µg h^{-1} in

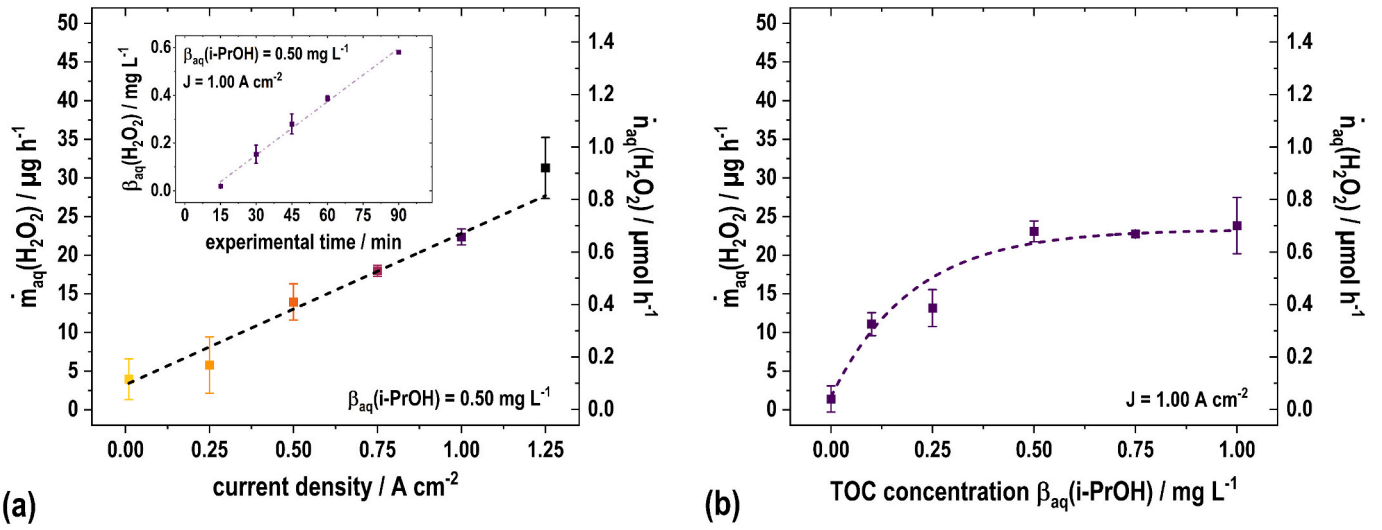

Fig. 7. Formation of H_2O_2 during electrochemical ozonation of aqueous solutions containing defined levels of i-PrOH. **(a)** Over the course of 90 min, a linear increase in H_2O_2 concentration can be measured in the reaction vessel when treating a 0.50 mg L^{-1} i-PrOH solution at a current density of 1.00 A cm^{-2} (inset graph). **(b)** For a fixed current density of J = 1.00 A cm^{-2}, a variation of TOC concentration leads to an increase in H_2O_2 production until plateauing at approx. 23 µg h^{-1}.

stand-by operation up to 31.2 ± 3.9 mg h^{-1} for J = 1.25 A cm^{-2}. The obtained slope of 7.46 µg L^{-1} min^{-1} equals a formation rate of 22.4 µg h^{-1} for the given reaction vessel, which serves as a common reference point in both Fig. 7(a) and (b). By evaluating different current densities, a linear approximation for the H_2O_2 formation rate is obtained (R^2 = 0.978) and enables a confident estimation of H_2O_2 concentrations for different operational setpoints. Even in stand-by operation, trace amounts of H_2O_2 evolve due to a small protection current and therefore electrolyzer activity. However, it has been reported that linearity in electrochemical H_2O_2 evolution over longer periods of time is not necessarily given due to possible subsequent reactions such as oxidation to oxygen at certain electrode materials [72,73].

When the PEM electrolyzer is operated without adding i-PrOH to the reaction vessel, minimal amounts of H_2O_2 can still be detected in a range of 1.4 µg h^{-1}. This may result from traces of residual organic compounds within the ultrapure water used for preparation. However, as soon as dissolved organic matter (DOM) as a carbon source is deliberately introduced into the system, a notable increase in H_2O_2 levels is measured. Varying the TOC level at a constant current density of 1.00 A cm^{-2} leads to an increase of the H_2O_2 formation rate up to only 23 µg h^{-1} for i-PrOH concentrations ≥ 0.50 mg L^{-1} (Fig. 7(b)), indicating that the rate of i-PrOH oxidation and therefore H_2O_2 formation depends on the amount of dissolved organic matter. For higher concentrations of i-PrOH no significant increase in H_2O_2 evolution is observed, which is in accordance with previous findings [58].

3.3. Correlation of ORP signals with ROS concentrations

Conventionally, the oxidation-reduction potential (ORP) provides a viable sum parameter given by a mixed potential to describe the disinfection efficacy of a given water sample without distinguishing the actual ROS composition. Fig. 8 emphasizes this relationship by plotting the measured ORP signal as a function of different concentrations for individual ROS. Herein, an increase in O_3 concentration for a range from 0.0 to 1.0 mg L^{-1} is accompanied by a proportionate increase of the ORP signal between approx. 250 and 700 mV and can be described by a linear relationship. While a linear correlation between the O_3 concentration and the ORP signal can be approximated up to 1 µg L^{-1}, H_2O_2 concentrations below 1 mg L^{-1} are not reliably distinguishable.

O_3 dosages as low as 0.2 mg L^{-1} are known to provide sufficient oxidative strength for process water sanitization and yield ORP signals of only approx. 350 mV. However, due to the strong pH dependence of

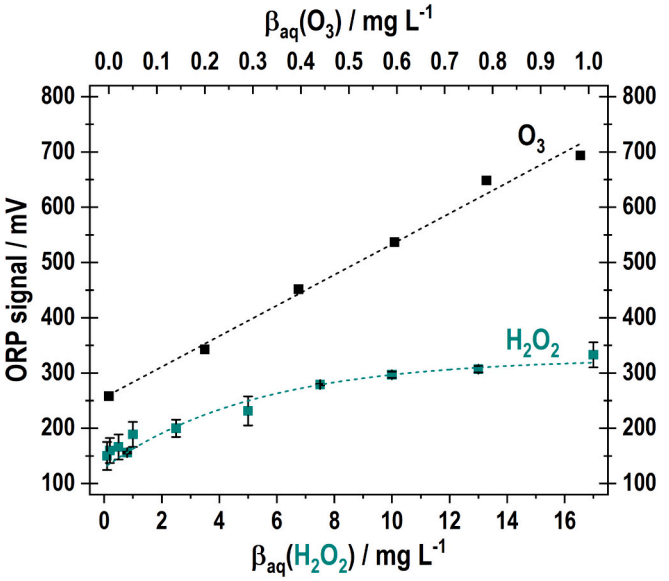

Fig. 8. Signal of a Pt ORP electrode as a function of the dissolved O_3 (black) or H_2O_2 (turquiose) concentration.

the ORP value, even moderate changes in pH might be sufficient to mask significant differences in the ROS composition. Furthermore, the presence of other species with a reducing potential interferes with the ORP value [74,75]. Considering the presented setup, cathodically produced hydrogen gas evolves in the same reaction vessel and can thus lower the measured potential at a conventional Pt ORP electrode. Unless the simultaneous occurrance of ROS and hydrogen can be prevented (*e.g.* by a suitable cell design), ORP electrodes with Au surfaces may be used as an alternative since they show a lower interaction with H_2.

Furthermore, an external calibration of sensors is often not sufficiently performed in field or long-term applications, which impairs a sensible interpretation of the ORP reading. For example, an ORP level of 350 mV may also be achieved with a H_2O_2 concentration level of 17 mg L^{-1}, which equals two orders of magnitude of higher oxidant dosage. As shown in this study however, this constitutes no reasonable level expected for the intended application in ultrapure water production and storage systems.

A further increase in ORP signal could not be realized within the observed concentration range by the application of additional H_2O_2 alone. Hence, if the ORP signal is considered as a preferred parameter for water quality, disinfection *via* H_2O_2 would require significantly higher oxidant concentrations. Moreover, a reliable estimation of low H_2O_2 concentrations by means of evaluating the ORP signal appears challenging and would not be associated with a noticeable disinfection performance either [76].

In systems where different reactive oxygen species can react with each other, the ORP signal is not a mere cumulative value. Fig. 9 depicts the effect of added H_2O_2 to an aqueous O_3 solution on the measured ORP signal.

During ozonation of ultrapure water samples, a steady disinfection performance can be monitored by a near constant ORP signal (Fig. 9(a)). Immediately upon H_2O_2 addition, the potential drops for a few minutes and stabilises at a considerably lower level after 5 to 10 min. This change in ORP provides a signal drop $\Delta U_{ORP,}$ which can be attributed to O_3 degradation *via* the fast peroxone process that is initiated when H_2O_2 is added to the O_3 solution [30]. While low amounts of added H_2O_2 coincide with low ΔU_{ORP} values, signal drops of up to 620 mV can be measured with H_2O_2 in broad excess ($n_0(H_2O_2)/n_0(O_3) = 13.5$). In these cases a pronounced decrease in pH of up to 0.5 units is observed, while experiments with a lower overall oxidant concentration are accompanied by almost insignificant changes in pH ($\Delta pH \leq 0.05$). In pretrials, it was possible to rule out that this effect is caused by minor amounts of phosphoric acid as a common stabilizing agent in H_2O_2 solutions. However, both these potentiometric measurements are limited with respect to their accuracy in ultrapure water due to the extremely low conductivity of the surrounding medium.

Since the ORP value changes with pH, comparing the effect of different ROS compositions is only meaningful referring to equal pH environments. As under the given experimental conditions O_3 constitutes the main oxidant contributing to the ORP value, the Nernst equation for its redox behavior can be employed to account for the observed change in pH [77] and approximate a correction function for the measured raw ORP values (Eq. (4)). While this correction is only of minor importance in ideal ultrapure water environments, it may be of high significance in other media.

$$\Delta U_{ORP} = \Delta U_{ORP,measured} + 59\ mV \cdot \Delta pH \quad (4)$$

From Fig. 9(b) it can be noted that the ORP signal drop increases with an increasing amount of H_2O_2 compared to the dissolved O_3, until it reaches a plateau as indicated by piecewise linear functions. This transition region occurs at $n_0(H_2O_2)/n_0(O_3) \approx 2.2$ for the 100 µg L^{-1} O_3 solution (grey bar) and at $n_0(H_2O_2)/n_0(O_3) \approx 0.85$ for the 50 µg L^{-1} solution (purple bar).

4. Conclusion

This study addresses the formation of O_3, ·OH and H_2O_2 during the operation of an electrolytic O_3 generator for ultrapure water disinfection. For all reactive oxygen species, the suitability of colorimetric detection assays based on DPD, HTA and $TiOSO_4$ was evaluated to quantify the respective cross-sensitivities among each other through linear calibration functions. Thus, a stepwise approach was proposed in order to determine the real concentration of all three ROS under investigation and to enable a predictive assessment of ROS evolution.

Specifically, we demonstrated that elevated formation rates for dissolved O_3 are only obtained when the applied current density exceeds 0.50 A cm^{-2}. Conversely, the formation of •OH due to O_3 decay shows a direct correlation among the entire current density range under investigation. Even minor quantities of dissolved organic carbon result in the observable generation of H_2O_2. By knowing the concentration of dissolved i-PrOH (given as the TOC level), the formation rate of H_2O_2 can be directly estimated based on the applied current density. However, when the TOC level surpasses 0.50 mg L^{-1}, no further increase in the formation rate of H_2O_2 occurs, remaining steady at 23 µg h^{-1} for J = 1.00 A cm^{-2}.

Considering that even low concentrations of produced H_2O_2 are capable of strongly affecting the O_3 content and eventually the ORP reading, the underlying TOC level and composition constitute a crucial parameter for ultrapure water ozonation. If neglected, unnecessarily high amounts of O_3 need to be produced to destroy residual organic matter, thus, distinct attention must be paid to monitoring the feed water quality. In consequence, this allows for future studies to focus on the development of spatially and time-resolved analyses of ROS in ultrapure water storage and distribution systems. Additional research

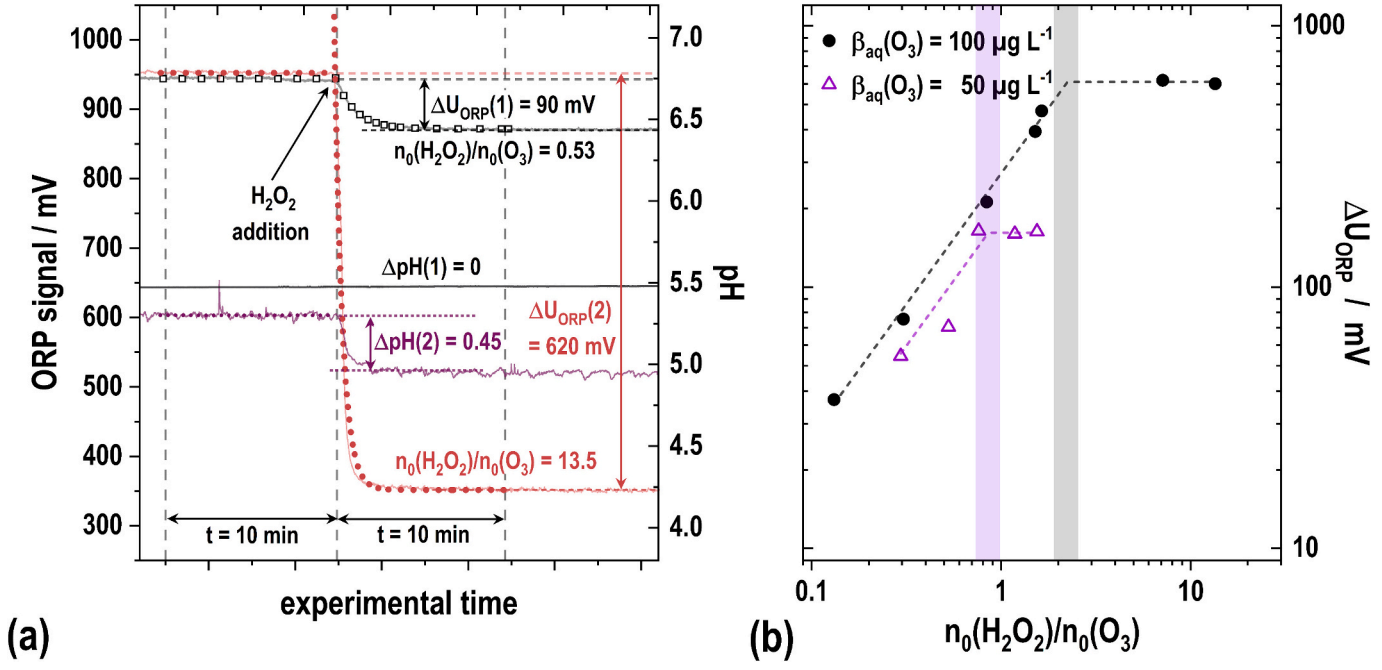

Fig. 9. **(a)** Effect of H_2O_2 on the ORP value of two exemplary O_3 solutions. **(b)** Effect of the $n_0(H_2O_2)/n_0(O_3)$ ratio on the ORP signal drop for different O_3 levels.

could be directed at the disinfection of natural waters by means of membrane electrolysis in the presence of a higher amount of dissolved minerals accompanied by an increased abundance of DOM.

Supplementary data to this article can be found online at https://doi.org/10.1016/j.jwpe.2024.105623.

CRediT authorship contribution statement

Roman Grimmig: Writing – original draft, Visualization, Methodology, Investigation, Formal analysis, Data curation, Conceptualization. **Philipp Gillemot:** Writing – original draft, Visualization, Formal analysis, Conceptualization. **Axel Kretschmer:** Investigation, Data curation. **Klaus Günther:** Writing – review & editing, Supervision. **Helmut Baltruschat:** Writing – review & editing, Supervision. **Steffen Witzleben:** Writing – review & editing, Supervision, Resources, Funding acquisition.

Declaration of competing interest

The authors declare the following financial interests/personal relationships which may be considered as potential competing interests:

Roman Grimmig works as an analytical chemist in the research and development department at Innovatec Gerätetechnik GmbH who provided the O_3 generators used and characterized in this study. All experiments and evaluations were performed independently and were not funded by Innovatec Gerätetechnik GmbH.

Data availability

Data will be made available on request.

Acknowledgements

The authors gratefully acknowledge the support by Dr. Samuel Stucki for helpful discussions. The authors would further like to express their thanks to Philipp Schmidt (Bonn-Rhein-Sieg University of Applied Sciences) for assistance in the lab and Amelia Heiner (Department of Material Science and Engineering, University of Utah, Salt Lake City, UT, USA) for proofreading.

Funding

This work was supported and financed by the Federal Ministry of Education and Research program “FHprofUnt” project “ReDeX” (grant number: 13FH107PX8).

References

[1] European Pharmacopeia, 9th ed., 2017.
[2] United States Pharmacopoeia, Water for Pharmaceutical Purposes <1231>, USP 40 - NF35, 2017.
[3] M. Bourgin, E. Borowska, J. Helbing, J. Hollender, H.P. Kaiser, C. Kienle, C. S. McArdell, E. Simon, U. von Gunten, Effect of operational and water quality parameters on conventional ozonation and the advanced oxidation process O3/H2O2: kinetics of micropollutant abatement, transformation product and bromate formation in a surface water, Water Res. 122 (2017) 234–245, https://doi.org/10.1016/j.watres.2017.05.018.
[4] D.B. Miklos, C. Remy, M. Jekel, K.G. Linden, J.E. Drewes, U. Hübner, Evaluation of advanced oxidation processes for water and wastewater treatment – a critical review, Water Res. 139 (2018) 118–131, https://doi.org/10.1016/j.watres.2018.03.042.
[5] Á. Moratalla, S.E. Correia, E. Lacasa, P. Murillo, P. Cañizares, M.A. Rodrigo, C. Sáez, Facing the treatment of polymedicated effluents using gaseous ozone electrochemically generated, J. Water Process Eng. 55 (2023), https://doi.org/10.1016/j.jwpe.2023.104153.
[6] W. Ding, S. Cao, W. Jin, X. Zhou, C. Wang, Q. Jiang, H. Huang, R. Tu, S.-F. Han, Q. Wang, Ozone disinfection of chlorine-resistant bacteria in drinking water, Water Res. 160 (2019) 339–349, https://doi.org/10.1016/j.watres.2019.05.014.
[7] S. Stucki, D. Schulze, D. Schuster, C. Stark, Ozonization of purified water systems, Pharm. Eng. 25 (2005) 40–56. http://apaco.ch.futura.ch-meta.net/xp_wysiwyg_media/jspe2005vol25no1_ozonization-of-purified-water-systems.pdf.
[8] L.M. Da Silva, M.H.P. Santana, J.F.C. Boodts, Electrochemistry and green chemical processes: electrochemical ozone production, Quim Nova 26 (2003) 880–888, https://doi.org/10.1590/s0100-40422003000600017.
[9] Z. Zhang, G. Yi, P. Li, X. Wang, X. Wang, C. Zhang, Y. Zhang, Recent progress in engineering approach towards the design of PbO2-based electrodes for the anodic oxidation of organic pollutants, J. Water Process Eng. 42 (2021) 102173, https://doi.org/10.1016/j.jwpe.2021.102173.
[10] C.A. Martínez-Huitle, M.A. Quiroz, C. Comninellis, S. Ferro, A. De Battisti, Electrochemical incineration of chloranilic acid using Ti/IrO2, Pb/PbO2 and Si/BDD electrodes, Electrochim. Acta 50 (2004) 949–956, https://doi.org/10.1016/j.electacta.2004.07.035.
[11] A. Kapałka, H. Baltruschat, C. Comninellis, Electrochemical Oxidation of Organic Compounds Induced by Electro-Generated Free Hydroxyl Radicals on BDD Electrodes, in: Synth, Diam. Film. Prep. Electrochem. Charact. Appl, John Wiley & Sons, Ltd, Hoboken, 2011, pp. 237–260, https://doi.org/10.1002/9781118062364.ch10.
[12] R. Amadelli, A.B. Velichenko, Lead dioxide electrodes for high potential anodic processes, J. Serbian Chem. Soc. 66 (2001) 836–845, https://doi.org/10.2298/JSC012835A.
[13] H. Ito, T. Maeda, A. Nakano, H. Takenaka, Properties of Nafion membranes under PEM water electrolysis conditions, Int. J. Hydrog. Energy 36 (2011) 10527–10540, https://doi.org/10.1016/j.ijhydene.2011.05.127.
[14] M. Paidar, V. Fateev, K. Bouzek, Membrane electrolysis—History, current status and perspective, Electrochim. Acta 209 (2016) 737–756, https://doi.org/10.1016/j.electacta.2016.05.209.
[15] F. Okada, K. Naya, Electrolysis for Ozone Water Production, in: Electrolysis, InechOpen, Rijeka, 2012, https://doi.org/10.5772/51945.
[16] C. Comninellis, Electrocatalysis in the Electrochemical Conversion/Combustion of Organic Pollutants for Waste Water Treatment, Electrochim. Acta 39 (1994) 1857–1862, https://doi.org/10.1016/0013-4686(94)85175-1.
[17] S. Stucki, G. Theis, R. Kötz, H. Devantay, H.J. Christen, In Situ Production of Ozone in Water Using a Membrel Electrolyzer, J. Electrochem. Soc. 132 (1985) 367–371, https://doi.org/10.1149/1.2113840.
[18] Y. Honda, T.A. Ivandini, T. Watanabe, K. Murata, Y. Einaga, An electrolyte-free system for ozone generation using heavily boron-doped diamond electrodes, Diam. Relat. Mater. 40 (2013) 7–11, https://doi.org/10.1016/j.diamond.2013.09.001.
[19] R. Grimmig, P. Gillemot, S. Lindner, P. Schmidt, S. Stucki, K. Günther, H. Baltruschat, S. Witzleben, Evaluating Platinum-Based Ionic Polymer Metal Composites as Potentiometric Sensors for Dissolved Ozone in Ultrapure Water Systems, Adv. Mater. Technol. 2202043 (2023) 1–13, https://doi.org/10.1002/admt.202202043.
[20] K. Sehested, H. Corfitzen, J. Holcman, E.J. Hart, On the mechanism of the decomposition of acidic O3 solutions, thermally or H2O2-initiated, J. Phys. Chem. A 102 (1998) 2667–2672, https://doi.org/10.1021/jp9721053.
[21] J. Staehelin, J. Hoigne, Decomposition of ozone in water in the presence of organic solutes acting as promoters and inhibitors of radical chain reactions, Environ. Sci. Technol. 19 (1985) 1206–1213, https://doi.org/10.1021/es00142a012.
[22] G. Merényi, J. Lind, S. Naumov, C. Von Sonntag, Reaction of ozone with hydrogen peroxide (peroxone process): a revision of current mechanistic concepts based on thermokinetic and quantum-chemical considerations, Environ. Sci. Technol. 44 (2010) 3505–3507, https://doi.org/10.1021/es100277d.
[23] D.A. Armstrong, R.E. Huie, W.H. Koppenol, S.V. Lymar, G. Merenyi, P. Neta, B. Ruscic, D.M. Stanbury, S. Steenken, P. Wardman, Standard electrode potentials involving radicals in aqueous solution: inorganic radicals (IUPAC Technical Report), Pure Appl. Chem. 87 (2015) 1139–1150, https://doi.org/10.1515/pac-2014-0502.
[24] A. Stefanova, S. Ayata, A. Erem, S. Ernst, H. Baltruschat, Mechanistic studies on boron-doped diamond: oxidation of small organic molecules, Electrochim. Acta 110 (2013) 560–569, https://doi.org/10.1016/j.electacta.2013.05.104.
[25] C.J. Bondue, P. Königshoven, H. Baltruschat, A New 2-Compartment Flow Through Cell for the Simultaneous Detection of Electrochemical Reaction Products by a Detection Electrode and Mass Spectroscopy, Electrochim. Acta 214 (2016) 241–252, https://doi.org/10.1016/j.electacta.2016.08.008.
[26] S. Garcia-Segura, E. Mostafa, H. Baltruschat, Electrogeneration of inorganic chloramines on boron-doped diamond anodes during electrochemical oxidation of ammonium chloride, urea and synthetic urine matrix, Water Res. 160 (2019) 107–117, https://doi.org/10.1016/j.watres.2019.05.046.
[27] E. Reisz, C. von Sonntag, A. Tekle-Röttering, S. Naumov, W. Schmidt, T.C. Schmidt, Reaction of 2-propanol with ozone in aqueous media, Water Res. 128 (2018) 171–182, https://doi.org/10.1016/j.watres.2017.10.035.
[28] J.J. Wu, J.S. Yang, M. Muruganandham, C.C. Wu, The oxidation study of 2-propanol using ozone-based advanced oxidation processes, Sep. Purif. Technol. 62 (2008) 39–46, https://doi.org/10.1016/j.seppur.2007.12.018.
[29] S.H. Schäfer, K. van Dyk, J. Warmer, T.C. Schmidt, P. Kaul, A New Setup for the Measurement of Total Organic Carbon in Ultrapure Water Systems, Sensors 22 (2022), https://doi.org/10.3390/s22052004.
[30] J. Staehelin, J. Hoigné, Decomposition of Ozone in Water: rate of Initiation by Hydroxide Ions and Hydrogen Peroxide, Environ. Sci. Technol. 16 (1982) 676–681, https://doi.org/10.1021/es00104a009.
[31] R.-F. Yu, H.-W. Chen, W.-P. Cheng, P.-H. Hsieh, Dosage Control of the Fenton Process for Color Removal of Textile Wastewater Applying ORP Monitoring and Artificial Neural Networks, J. Environ. Eng. 135 (2009) 325–332, https://doi.org/10.1061/(asce)ee.1943-7870.0000016.
[32] U. Feistel, P. Otter, S. Kunz, T. Grischek, J. Feller, Field tests of a small pilot plant for the removal of arsenic in groundwater using coagulation and filtering, J. Water Process Eng. 14 (2016) 77–85, https://doi.org/10.1016/j.jwpe.2016.10.006.

[33] P. Kruse, Review on water quality sensors, J. Phys. D. Appl. Phys. 51 (2018) 203002, https://doi.org/10.1088/1361-6463/aabb93.
[34] E.S. Massima Mouele, O.O. Fatoba, O. Babajide, K.O. Badmus, L.F. Petrik, Review of the methods for determination of reactive oxygen species and suggestion for their application in advanced oxidation induced by dielectric barrier discharges, Environ. Sci. Pollut. Res. 25 (2018) 9265–9282, https://doi.org/10.1007/s11356-018-1392-9.
[35] P. Fernández-Castro, M. Vallejo, M.F. San Román, I. Ortiz, Insight on the fundamentals of advanced oxidation processes: role and review of the determination methods of reactive oxygen species, J. Chem. Technol. Biotechnol. 90 (2015) 796–820, https://doi.org/10.1002/jctb.4634.
[36] R. Knake, P.C. Hauser, Sensitive electrochemical detection of ozone, Anal. Chim. Acta 459 (2002) 199–207, https://doi.org/10.1016/S0003-2670(02)00121-6.
[37] W.R. Penrose, L. Pan, J.R. Stetter, W.M. Ollison, Sensitive measurement of ozone using amperometric gas sensors, Anal. Chim. Acta 313 (1995) 209–219, https://doi.org/10.1016/0003-2670(95)00251-T.
[38] H. Bader, J. Hoigné, Determination of ozone in water by the indigo method, Water Res. 15 (1981) 449–456, https://doi.org/10.1016/0043-1354(81)90054-3.
[39] J. Nobbs, C. Tizaoui, A Modified Indigo Method for the Determination of Ozone in Nonaqueous Solvents, Ozone Sci. Eng. 36 (2014) 110–120, https://doi.org/10.1080/01919512.2013.836956.
[40] A.T. Palin, Current DPD methods for residual halogen compounds and ozone in water, J. Am. Water Works Assoc. 67 (1975) 32–33, https://doi.org/10.1002/j.1551-8833.1975.tb02149.x.
[41] DIN 38408-3:2011-04, Deutsche Einheitsverfahren zur Wasser-, Abwasser- und Schlammuntersuchung - Gasförmige Bestandteile (Gruppe G) - Teil 3: Bestimmung von Ozon (G 3), 2011.
[42] P. Zhu, R. Wu, X. Liu, Z. Yang, P. Xu, B. Hou, Rapid measurement of trace periodate concentration with bromide ion–catalyzed periodate for oxidation colorization of DPD, J. Water Process Eng. 58 (2024) 104825, https://doi.org/10.1016/j.jwpe.2024.104825.
[43] J. Zou, H. Cai, D. Wang, J. Xiao, Z. Zhou, B. Yuan, Spectrophotometric determination of trace hydrogen peroxide via the oxidative coloration of DPD using a Fenton system, Chemosphere 224 (2019) 646–652, https://doi.org/10.1016/j.chemosphere.2019.03.005.
[44] G. Louit, S. Foley, J. Cabillic, H. Coffigny, F. Taran, A. Valleix, J.P. Renault, S. Pin, The reaction of coumarin with the OH radical revisited: hydroxylation product analysis determined by fluorescence and chromatography, Radiat. Phys. Chem. 72 (2005) 119–124, https://doi.org/10.1016/j.radphyschem.2004.09.007.
[45] M.D.G. de Luna, J.I. Colades, C.C. Su, M.C. Lu, Comparison of dimethyl sulfoxide degradation by different Fenton processes, Chem. Eng. J. 232 (2013) 418–424, https://doi.org/10.1016/j.cej.2013.07.107.
[46] R.S. Lankone, A.R. Deline, M. Barclay, D.H. Fairbrother, UV–Vis quantification of hydroxyl radical concentration and dose using principal component analysis, Talanta 218 (2020) 121148, https://doi.org/10.1016/j.talanta.2020.121148.
[47] T. Deng, S. Hu, X. An Huang, J. Song, Q. Xu, Y. Wang, F. Liu, A novel strategy for colorimetric detection of hydroxyl radicals based on a modified Griess test, Talanta 195 (2019) 152–157, https://doi.org/10.1016/j.talanta.2018.11.044.
[48] Z. Li, S. Yuan, C. Qiu, Y. Wang, X. Pan, J. Wang, C. Wang, J. Zuo, Electrochimica Acta Effective degradation of refractory organic pollutants in landfill leachate by electro-peroxone treatment, Electrochim. Acta 102 (2013) 174–182, https://doi.org/10.1016/j.electacta.2013.04.034.
[49] X. Sui, X. Duan, F. Xu, L. Chang, Journal of the Taiwan Institute of Chemical Engineers Fabrication of three-dimensional networked PbO 2 anode for electrochemical oxidation of organic pollutants in aqueous solution, J. Taiwan Inst. Chem. Eng. 100 (2019) 74–84, https://doi.org/10.1016/j.jtice.2019.04.007.
[50] Y. Arbid, M. Usman, N.T. Luong, B. Mathon, B. Cedat, J.-F. Boily, K. Hanna, Use of iron-bearing waste materials in laundry wastewater treatment, J. Water Process Eng. 57 (2024) 104717, https://doi.org/10.1016/j.jwpe.2023.104717.
[51] S. Pei, S. You, J. Ma, X. Chen, N. Ren, Electron Spin Resonance Evidence for Electro-generated Hydroxyl Radicals, Environ. Sci. Technol. 54 (2020) 13333–13343, https://doi.org/10.1021/acs.est.0c05287.
[52] E. Kurowska, A. Brzózka, M. Jarosz, G.D. Sulka, M. Jaskuła, Silver nanowire array sensor for sensitive and rapid detection of H2O2, Electrochim. Acta 104 (2013) 439–447, https://doi.org/10.1016/j.electacta.2013.01.077.
[53] L. Domínguez-Henao, A. Turolla, D. Monticelli, M. Antonelli, Assessment of a colorimetric method for the measurement of low concentrations of peracetic acid and hydrogen peroxide in water, Talanta 183 (2018) 209–215, https://doi.org/10.1016/j.talanta.2018.02.078.
[54] J.L. Aquino de Queiroz, C.A. Martínez-Huitle, P.S. Castro, Real time monitoring of in situ generated hydrogen peroxide in electrochemical advanced oxidation reactors using an integrated Pt microelectrode, Talanta 218 (2020) 121133, https://doi.org/10.1016/j.talanta.2020.121133.
[55] G.M. Eisenberg, Colorimetric Determination of Hydrogen Peroxide, Ind. Eng. Chem. Anal. Ed. 15 (1943) 327–328, https://doi.org/10.1021/i560117a011.
[56] G.A. Zoumpouli, M. Scheurer, H.J. Brauch, B. Kasprzyk-Hordern, J. Wenk, O. Happel, COMBI, continuous ozonation merged with biofiltration to study oxidative and microbial transformation of trace organic contaminants, Environ. Sci. Water Res. Technol. 5 (2019) 552–563, https://doi.org/10.1039/c8ew00855h.
[57] N. Hermes, G. Knupp, Transformation of atrazine, bisphenol A and chlorendic acid by electrochemically produced oxidants using a lead dioxide electrode, Environ. Sci. Water Res. Technol. 1 (2015) 905–912, https://doi.org/10.1039/c5ew00149h.
[58] S. Stucki, H. Baumann, Application of Electrochemical Ozone Generators in Ultrapure Water Systems, in: Process Technol. Water Treat., Plenum Press, New York, 1988, pp. 191–201, https://doi.org/10.1007/978-1-4684-8556-1_19.
[59] J. Hoigné, Inter-calibration of OH radical sources and water quality parameters, Water Sci. Technol. 35 (1997) 1–8, https://doi.org/10.1016/S0273-1223(97)00002-4.
[60] DIN 38409-15:1987-06, Deutsche Einheitsverfahren zur Wasser-, Abwasser- und Schlammuntersuchung; Summarische Wirkungs- und Stoffkenngrößen (Gruppe H); Bestimmung von Wasserstoffperoxid (Hydrogenperoxid) und seinen Addukten (H 15), 1987.
[61] J.P. Crow, C. Spruell, J. Chen, C. Gunn, H. Ischiropoulos, M. Tsai, C.D. Smith, R. Radi, W.H. Koppenol, J.S. Beckman, On the pH-dependent yield of hydroxyl radical products from peroxynitrite, Free Radic. Biol. Med. 16 (1994) 331–338, https://doi.org/10.1016/0891-5849(94)90034-5.
[62] H. Shiraishi, M. Kataoka, Y. Morita, J. Umemoto, Interactions of Hydroxyl Radicals with Tris (Hydroxymethyl) Aminomethane and Good's Buffers Containing Hydroxymethyl or Hydroxyethyl Residues Produce Formaldehyde, Free Radic. Res. Commun. 19 (1993) 315–321, https://doi.org/10.3109/10715769309056520.
[63] V.M. Mishin, P.E. Thomas, Characterization of hydroxyl radical formation by microsomal enzymes using a water-soluble trap, terephthalate, Biochem. Pharmacol. 68 (2004) 747–752, https://doi.org/10.1016/j.bcp.2004.05.004.
[64] M.A. Rosenfeld, S.D. Razumovskii, A.N. Shchegolikhin, M.L. Konstantinova, N. B. Sultimova, A.I. Kozachenko, L.G. Nagler, A.V. Bychkova, V.B. Leonova, Nature of active intermediate particles formed during ozone-induced oxidation, Dokl. Biochem. Biophys. 461 (2015) 139–141, https://doi.org/10.1134/S1607672915020180.
[65] J. Steidtner, F. Hernandez, H. Baltruschat, Electrocatalytic reactivity of Pd monolayers and monatomic chains on Au, J. Phys. Chem. C 111 (2007) 12320–12327, https://doi.org/10.1021/jp071712f.
[66] C. von Sonntag, U. von Gunten, Chemistry of Ozone in Water and Wastewater Treatment: From Basic Principles to Applications, IWA Publishing, London, 2012, https://doi.org/10.2166/9781780400839.
[67] S. Stucki, H. Baumann, H.J. Christen, R. Kötz, Performance of a pressurized electrochemical ozone generator, J. Appl. Electrochem. (1987), https://doi.org/10.1007/BF01007814.
[68] Y. Jing, B.P. Chaplin, Mechanistic Study of the Validity of Using Hydroxyl Radical Probes to Characterize Electrochemical Advanced Oxidation Processes, Environ. Sci. Technol. 51 (2017) 2355–2365, https://doi.org/10.1021/acs.est.6b05513.
[69] M. Panizza, G. Cerisola, Electrocatalytic materials for the electrochemical oxidation of synthetic dyes, Appl. Catal. B Environ. 75 (2007) 95–101, https://doi.org/10.1016/j.apcatb.2007.04.001.
[70] S. Lim, J.L. Shi, U. von Gunten, D.L. McCurry, Ozonation of organic compounds in water and wastewater: a critical review, Water Res. 213 (2022) 118053, https://doi.org/10.1016/j.watres.2022.118053.
[71] G.V. Buxton, C.L. Greenstock, W.P. Helman, A.B. Ross, Critical review of rate constants for reactions of hydrated electrons, hydrogen atoms and hydroxyl radicals (·OH/·O− in aqueous solution), J. Phys. Chem. Ref. Data 17 (1988) 513–886, https://doi.org/10.1063/1.555805.
[72] B. Marselli, J. Garcia-Gomez, P.-A. Michaud, M.A. Rodrigo, C. Comninellis, Electrogeneration of Hydroxyl Radicals on Boron-Doped Diamond Electrodes, J. Electrochem. Soc. 150 (2003) D79, https://doi.org/10.1149/1.1553790.
[73] I. Kisacik, A. Stefanova, S. Ernst, H. Baltruschat, Oxidation of carbon monoxide, hydrogen peroxide and water at a boron doped diamond electrode: the competition for hydroxyl radicals, Phys. Chem. Chem. Phys. 15 (2013) 4616–4624, https://doi.org/10.1039/c3cp44643c.
[74] C.M. Pham, N.Q. Pham, A.K. Le, Oxidation-Reduction Potential and Peroxone Process in Antibiotic Residues Removal from Hospital Wastewater, Chem. Eng. Trans. 97 (2022) 187–192, https://doi.org/10.3303/CET2297032.
[75] T.W. LeBaron, R. Sharpe, ORP should not be used to estimate or compare concentrations of aqueous H2: an in silico analysis and narrative synopsis, Front, Food Sci. Technol. 2 (2022) 1–17, https://doi.org/10.3389/frfst.2022.1007001.
[76] C. Kim, Y.C. Hung, R.E. Brackett, Roles of oxidation-reduction potential in electrolyzed oxidizing and chemically modified water for the inactivation of food-related pathogens, J. Food Prot. 63 (2000) 19–24, https://doi.org/10.4315/0362-028X-63.1.19.
[77] S. Okouchi, M. Suzuki, K. Sugano, S. Kagamimori, S. Ikeda, Water desirable for the human body in terms of oxidation-reduction potential (ORP) to pH relationship, J. Food Sci. 67 (2002) 1594–1598, https://doi.org/10.1111/j.1365-2621.2002.tb08689.x.
[78] D. Rosestolato, R. Amadelli, A.B. Velichenko, Electrode characteristics for ozone production: a case study using undoped and doped PbO2 on porous platinised titanium substrates, J. Solid State Electrochem. 20 (2016) 1181–1190, https://doi.org/10.1007/s10008-015-2945-1.
[79] F.J. Beltran, Ozone Reaction Kinetics for Water and Wastewater Systems, Lewis Publishers, Boca Raton, 2003, https://doi.org/10.1201/9780203509173.
[80] B. Langlais, D.A. Reckhow, D.R. Brink, Ozone in Water Treatment: Application and Engineering, Lewis Publishers, Routledge, 1991, https://doi.org/10.2134/jeq1991.00472425002000040040x.
[81] A.N. Ignatiev, A.N. Pryakhin, V.V. Lunin, Numerical simulation of the kinetics of ozone decomposition in an aqueous solution, Russ. Chem. Bull. 57 (2008) 1172–1178, https://doi.org/10.1007/s11172-008-0146-0.
[82] I. Fábián, Reactive intermediates in aqueous ozone decomposition: a mechanistic approach, Pure Appl. Chem. 78 (2006) 1559–1570, https://doi.org/10.1351/pac200678081559.